Journal of Colloid and Interface Science 410 (2013) 152–157

Contents lists available at ScienceDirect

Journal of Colloid and Interface Science

www.elsevier.com/locate/jcis

Vertically-aligned Prussian blue/carbon nanotube nanocomposites on a carbon microfiber as a biosensing scaffold for ultrasensitively detecting glucose

Kuanping Gong

San Jose Lab, Corporate Research Institute, Samsung Cheil Industries Inc., San Jose, CA 95131, United States

ARTICLE INFO

Article history:
Received 27 May 2013
Accepted 1 August 2013
Available online 14 August 2013

Keywords:
Prussian blue
Carbon nanotube
Nanoelectrode array
Glucose biosensor

ABSTRACT

We describe our assembly and the analytical performance of a glucose biosensor consisting of an array of carbon nanotubes (CNTs) that perpendicularly fall on a 7-μm-diameter carbon fiber and are modified by a "dual" enzymatic system—*viz.* glucose oxidase (GOx) and Prussian blue (PB, an *artificial peroxidase*). We chose to use the PB-catalyzed reduction reaction of hydrogen peroxide, an end-product of the GOx-catalyzed oxidation of glucose, to "relay" electrons from GOx to the substrate electrode. We highlight that the electrode-structural alignment of this novel biosensing system plays a crucial role in optimizing the electrochemical- and catalytic-reactions of the enzymes with their substrates. The vertical alignment of enzyme-modified CNTs with the pores located between neighboring individual CNTs creates the simplest optimized pathways for substrates to diffuse to the enzymes and for the generated electrical signals to transport along the nanotube's length to an electronic analyzer. Consequently, the glucose biosensor thus constructed exhibits a high sensitivity of 4.9 μA/mM with a detection limit of 0.05 mmol/L and long-term stability in amperometrically detecting glucose. Our long-range-order assembling of electroactive biomolecules and microscale/nanoscale materials into a multifunctional biocomposite accounts for this superb performance of vital importance in their realistic applications in deciphering glucose and hydrogen peroxide.

1. Introduction

Today, more than 300 million people worldwide suffer from diabetes, causing ~5% of all deaths globally; the affected population is growing by 7 million each year [1]. The point-of-care tests to manage this disease challenge us to develop cost-effective sensors for reporting glucose precisely and rapidly. In this context, electrochemical glucose biosensors seemingly constitute a valuable stratagem that rests upon the high efficiency and specificity inherent in enzymatic reactions to transduce the information of interest in a target analyte into electrochemical signals [2–4]. Such bioelectro-analytical methods technically feature high performance and simple instrumentation that are invaluable for its widespread adoptions in clinic diagnoses and self-monitoring services [5,6]. However, difficulties arise when targeting enzyme-based biosensors: (i) The active centers of most enzymes, including glucose oxidase (GOx), are embedded deep in their multi-level folded structures [7], thereby complicating electrical communication between the enzymes and the substrate electrodes; (ii) ideally, every single enzyme molecule should be sited in a biocompatible, flexible environment with a large electrochemical surface area, especially when a high loading of enzymes must be used to amplify the output of electrochemical signals [6]; and (iii) many substrates of the glucose-redox enzymes have a very low concentration and diffusion coefficient, so that substrate-involved reactions may limit the overall kinetics [8].

Carbon nanotubes (CNTs) and their derivatives were heralded as ideally useful for devising such biosensors because their unique chemical- and structural-properties [6,8–10]—such as robust stability, excellent conductivity, and extremely high surface area—afford rationales to integrate them with biomolecules (e.g., proteins) into new multifunctional biocomposites [2–6]. Nevertheless, these properties were far too compromised to be well appreciated in CNT-based electrochemical biosensors, so far fabricated by the two major methods of preparing electrodes: drop-coating or spin-coating a CNT suspension on the surface of substrate electrodes [8,9]. These approaches often entail additional, zigzag pathways for electron transfer and mass diffusion, and/or insufficient bioactive sites accessible to substrates. Consequently, there is a notable limit to accessing the applicable potential of CNTs in developing electrochemical biosensors.

Here, we report on the essential role of electrode design in determining the biosensors' performance, in addition to the effect of the electrode materials themselves. To validate this concept, we

E-mail addresses: kuanping.gong@gmail.com, k.gong@samsung.com

0021-9797/$ - see front matter © 2013 Elsevier Inc. All rights reserved.
http://dx.doi.org/10.1016/j.jcis.2013.08.005

demonstrated the preparation and analytical performance of an electrochemical glucose biosensor consisting of a modified "dual" enzymatic system, with an array of vertically-aligned CNT nanobioelectrodes on a carbon microfiber. The "dual" enzymatic system encompasses GOx and Prussian blue (PB, $Fe_4[Fe(CN)_6]_3$); PB is termed an *artificial peroxidase* because of its analogy with the biological family of peroxidases in catalyzing the reduction in peroxides [11]. The dimension of the resultant electrode is on the micrometer scale, so sharing the microelectrode's intrinsic features, such as radial mass diffusion, high temporal- and spatial-resolution, and negligible ohmic drop [12,13].

2. Experimental section

2.1. Chemicals and materials

We purchased from Sigma the glucose oxidase (GOx, EC 1.1.3.4, 47,200 units/g, from *Aspergillus niger*), bovine serum albumin (BSA, lyophilized powder), glutaraldehyde, D-(+)-glucose, silicon tetrachloride, Nafion® (5 wt.% in ethanol/water mix), phthalocyanine, potassium ferricyanide ($K_3Fe(CN)_6$), and hydrogen peroxide (H_2O_2, 30%). All the chemicals were of analytical grade and were used as received. Glucose solution was prepared in a phosphate-buffered solution (pH 6.8) and stored overnight at 4 °C before use. We prepared all the aqueous solutions in double-distilled water. Carbon fibers were supplied by Fabric Development Inc..

2.2. Preparation of GOx/PB/VA-CNT/CFME

2.2.1. Synthesis of VA-CNT/CF composites

We produced vertically-aligned carbon nanotubes on a 7-μm-diameter carbon fiber, i.e., VA-CNT/CF, with a modification of the chemical-vapor-deposition method reported previously [14]. In brief, we first modified the surface of CFs with a thin layer of PB nanoparicles by the potential-stepping technique (*vide infra*). This pre-treated PB/CF was used as a support for growing CNTs by pyrolysis of phthalocyanine at 800 °C under a reducing atmosphere (H_2/Ar, 15:85 in volume).

2.2.2. Preparation of VA-CNT/CFME

We fabricated VA-CNT/CF microelectrodes (i.e., VA-CNT/CFME) according to methodology in a previous report with a slight modification [15]. Initially, we cut off a fragment of CNT/CF and connected it with silver epoxy to a copper wire in a head-to-tail way. After drying the heterojunction wire in air for 5 h, we carefully inserted it into a borosilicate glass tube (O.D., 1.5 mm; I.D., 0.86 mm; length: 10 cm), leaving 2–3 cm of the bottom end of the copper protruding from the tube. Then, we generated a CNT/CFME by pulling the borosilicate glass tube with a micropipette puller (P-30 Vertical, Sutter Instrument) before we cut the free tip-end of CNT/CF to form a 300–500 μm long piece out of the thus formed glass tip. The two ends of the formed glass tube were sealed with polystyrene to ensure stability.

2.2.3. Preparation of PB/VA-CNT/CFME

In 0.5 M KCl solution containing 5.0 mM $K_3Fe(CN)_6$ and 0.1 w/w% Nafion®, we repeatedly applied a rectangular potential (from 0.0 V to 1.3 V with the time steps of 5 and 10 s, respectively) to the CNT/CFME for growing PB nanoparticles on the nanotubes, forming PB/VA-CNT/CF microelectrodes (PB/VA-CNT/CFME).

2.2.4. Preparation of GOx/PB/VA-CNT/CFME bioseonsors

The enzyme electrode of GOx/PB/CNT/CFs was prepared by immersing the PB/VA-CNT/CFME in an enzyme solution consisting of 50.0 mg GOx, 25 mg BSA, and 25 μL glutaraldehyde for 1 h, followed by drying in air. For comparison, a GOx/PB/CFME was prepared by the same procedure.

2.3. Materials characterization

Scanning electron microscopy (SEM) imaging was performed on a Hitachi S4800 high-resolution SEM unit (Tokyo, Japan). For acquiring Raman spectra and optical images, we employed an inVia micro-Raman spectrometer (Renishaw) with an Ar ion laser of 785 nm wavelength. For the FT-IR measurements, the samples were pressed into a KBr pellet and then measured with a Spectrum One infrared spectrometer (PerkinElmer, Inc.).

2.4. Electrochemical measurements

Electrochemical measurements were conducted using a computer-controlled potentiostat (CHI 760C, Austin, USA) coupled with a conventional three-electrode system. The as-prepared various electrodes were used as working electrodes, an Ag/AgCl (3 M KCl-filled) electrode as reference electrode, and a platinum wire as the counter electrode. GOx/PB/VA-CNT/CFME and the GOx/PB/CFME (without CNTs) were used for *i–t* amperometric measurements at 0.0 V in 0.10 M PBS containing various concentrations of glucose. The solution was stirred with a magnetic stirrer at 800 rpm. Aliquots of glucose solution were pipetted, stepwise, into the solution, and the current response was recorded after a smooth background was obtained. All the electrochemical measurements were taken at room temperature (23 °C).

3. Results and discussion

3.1. Electrodeposition of PB nanoparticles on VA-CNT/CFME

We placed PB nanoparticles on the VA-CNT/CFME, forming PB/VA-CNT/CFME, by subjecting it to a rectangular potential in 0.5 M KCl electrolyte containing 5.0 mM $K_3Fe(CN)_6$ and 0.1 w/w% Nafion® (Fig. 1). The formation of PB on the VA-CNT/CFME was monitored with cyclic voltammetry in the same solution as used for

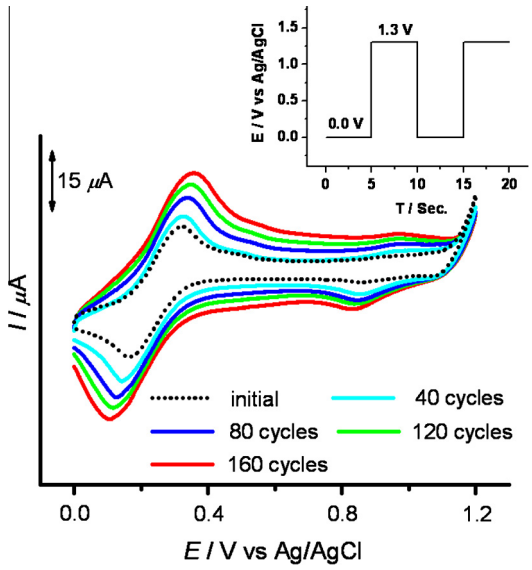

Fig. 1. CVs of the VA-CNT/CFME in 0.5 M KCl solution containing 5.0 mM $K_3Fe(CN)_6$ and 0.1 w/w% Nafion® after different cycles of the rectangular potential scanning in the same solution. Cycling number from innermost to outermost is 0, 40, 80, 120, and 160. Scan rate, 100 mV s^{-1}. The inset shows the rectangular potential applied for the electrodeposition of PB.

the electrochemical deposition. Fig. 1 shows the initial voltammogram of the CNT/CFME, *viz.* before electrochemical deposition (dotted, black curve), which records two peaks corresponding to the $Fe(CN)_6^{3-/4-}$ redox couple only. In contrast, two additional pairs of redox peaks centered, respectively, at 0.20 V and 0.80 V become apparent after applying the rectangular potential to the VA-CNT/CFME. Their current intensity gradually increased with the potential-step cycle until about 160 cycles. The first couple of peaks (around 0.20 V) overlapped with the peak of the $Fe(CN)_6^{3-/4-}$ species, as we confirmed with controlled experiments in the same solution lacking the $Fe(CN)_6^{3-/4-}$ species. This reversible procedure corresponds to the electrochemical transition between PB and Prussian White (PW, $K_2Fe^{II}[Fe^{II}(CN)_6]$). Further, the other couple of peaks (around 0.80 V) are characteristics of the transformation of PB and Prussian Yellow (PY, $Fe^{III}[Fe^{III}(CN)_6]$) [16–19]. Collectively, these electrochemical features indicate the successful growth of PB on the VA-CNT/CFME.

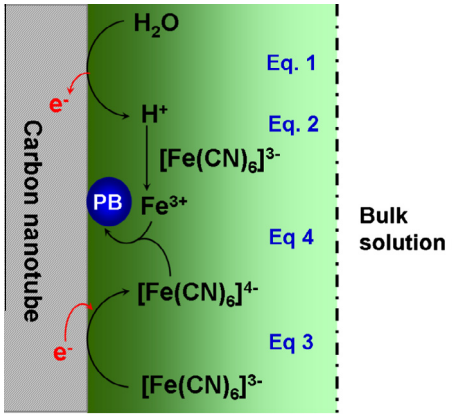

$$2H_2O \rightarrow O_2 + 4H^+ + 4e^- \quad (1.3\ V) \qquad \text{Equation 1}$$

$$6H^+ + [Fe(CN)_6]^{3-} \rightarrow 6HCN + Fe^{3+} \qquad \text{Equation 2}$$

$$[Fe(CN)_6]^{3-} + e^- \rightleftharpoons [Fe(CN)_6]^{4-} \quad (0.0\ V) \qquad \text{Equation 3}$$

$$K^+ + Fe^{3+} + [Fe(CN)_6]^{4-} \rightarrow KFe^{III}[Fe^{II}(CN)_6]\downarrow \qquad \text{Equation 4}$$

Fig. 2. Schematic illustration showing the electrochemical- and chemical-reactions at the vicinity of the VA-CNT/CFME upon subjecting it to the rectangular potential cycling (see Fig. 1).

PB can be synthesized by the complexation of ferric ions and hexacyanoferrate (II) that either are present in the solution or chemically generated as an intermediate [20,21]. In our synthesis, we chose to generate the ferric precursor ions by a combination of electrochemical- and chemical-reactions at the individual CNTs, as depicted by Eqs. (1) and (2) in Fig. 2. The ferric ions so produced have a relatively slow diffusion coefficient, and hence, they were "trapped" near the CNT surfaces within the short period of the potential-step time to react with hexacyanoferrate (II) in the following potential polarization at 0.0 V (Eqs. (3) and (4), Fig. 2). A high potential that is required to anchor Eq. (1) plays a vital role in this synthesis, since no PB was detected in cyclic voltammogram or in SEM imaging when the potential was switched beyond potentials high enough to generate protons. Eq. (1) does not occur at the PB nanoparticles under the same conditions, so that only at the CNT surface, PB can grow. Consequently, the newly formed individual PB nanoparticles were arranged along the CNTs' lengths, rather than overlapping another one, to form the monodispersed PB nanoparticles on the CNTs.

To confirm this proposed synthetic mechanism, we followed the same procedure under identical conditions using two different electrodes, a bare CFME and a glassy carbon electrode (GCE), to grow PB nanoparticles. We allowed an extended period (200 cycles) for the electrochemical deposition of PB to better validate the efficiency of this synthesis in attaining homogeneous, monodispersed PB nanoparticles on the CNTs. As Fig. 3 shows, we met our goal. These experimental results indicate that this method of electrochemical synthesis, coupled with the well-defined aligned electrode structure, allows us to assemble electroactive (bio)molecules and nanomaterial components into composites in a long-range-order way.

3.2. Characterization of PB/VA-CNT/CFME

The inset in Fig. 4A shows a representative Raman-imaging photograph of the PB/VA-CNT/CFME tip. The needle that protrudes

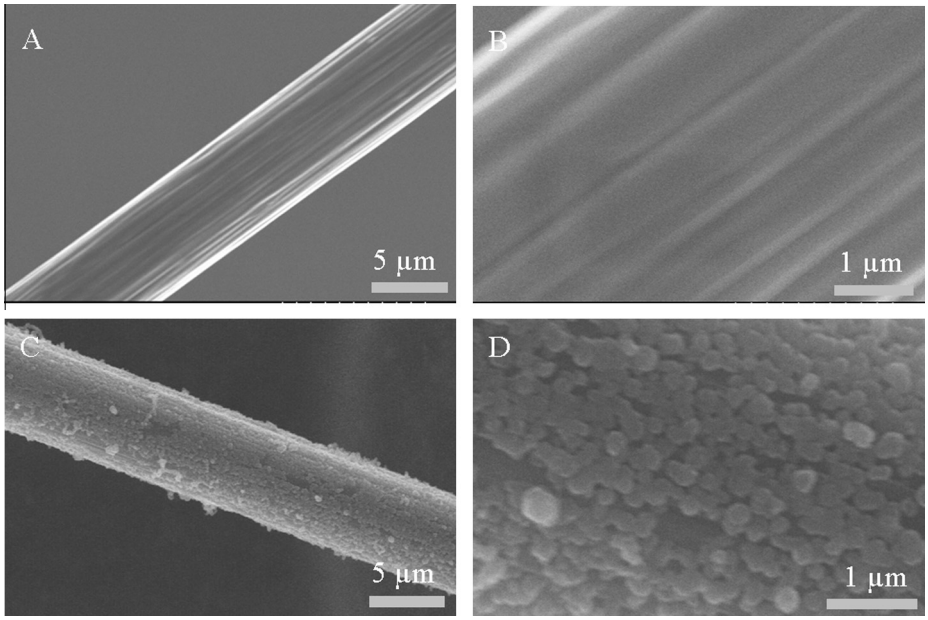

Fig. 3. Low- and higher-magnification SEM images for a bare CF (A and B) and PB/CF (C and D).

about 400 μm out of the glass tube's end is the active part of the as-prepared PB/VA-CNT/CFME. We sealed the two ends of the glass tube with polystyrene to ensure the electrode's mechanical- and electrochemical-stability, while collecting current to a potentiostat was accomplished via a copper wire whose tip was connected with the tailored-end of the PB/VA-CNT/CFME by silver epoxy. While Fig. 4A shows a top-down SEM image of the as-prepared PB/VA-CNT/CFME, Fig. 4B shows the counterpart morphology after we elaborately scratched the microelectrode along its length for convenience to visualize the orientation of CNTs. The nanotubes are closely packed and uniformly grown on a 7-μm-diameter fiber. More interestingly, we observed a well-defined array of vertically-aligned carbon nanotubes measuring about 10 μm in length that surrounds the curved surface of the microfiber. This observation was further confirmed by the corresponding cross-sectional SEM image, showing a defining hierarchical nanostructure consisting of a fiber and a coating of modified nanotubes in different scales of dimension (Fig. 4C). The higher magnification SEM image of the area squared in Fig. 4C reveals that nanoparticles averaging 40 nm are monodispersed along the nanotubes, lengths (Fig. 4D). We consider that the monodispersion of the particles on the nanotubes and their favorable interaction reflects our well-controlled synthesis, wherein the ferric-ion precursor is generated electrochemically only at the CNT's surfaces and confined to their vicinities within the period of the potential-step time. We envisaged this dependence by growing PB nanoparticles on a bare CF electrode in the same way, and consequently, monodispersed PB nanoparticles indeed were observed (Fig. 3). We also used the as-prepared electrode, PB/CFME, as a reference for comparison (*vide infra*).

We confirmed the successful deposition of PB on the CNTs by FT-IR and Raman spectroscopy, in addition to the cyclic-voltammetric evidence (Fig. S1). Fig. 5A shows a typical FT-IR spectrum for the PB/VA-CNT/CFME in parallel with those for its components, the CNTs and the PB nanoparticles. The CNT sample displays an IR-absorption band at 1580 cm^{-1} due to the υ(C=C) mode near the defect site [22]. The FT-IR spectrum of the PB sample shows two characteristic bands at 2070 cm^{-1} and 450–650 cm^{-1} that we

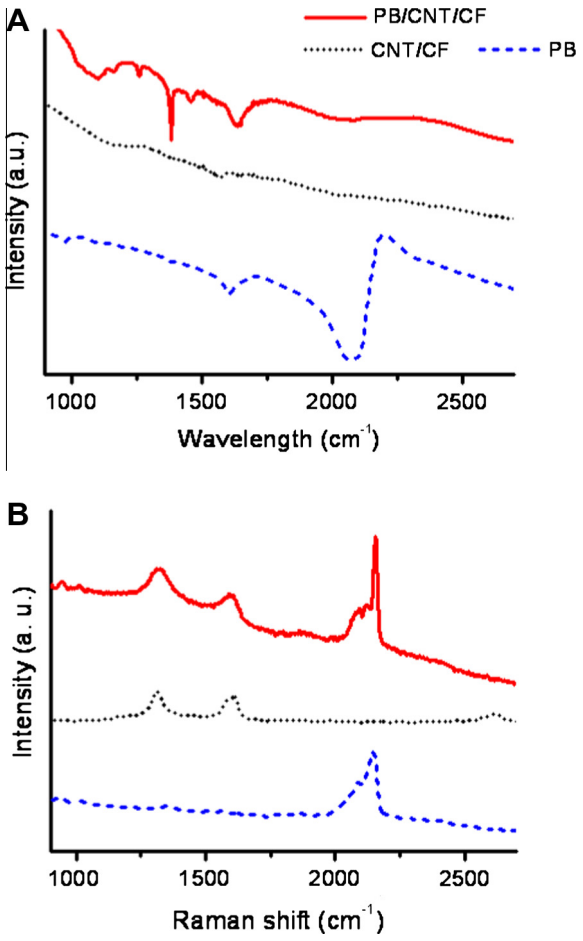

Fig. 5. FT-IR spectra (A) and first-order Raman spectra (B) for the VA-CNT/CF (upper, black), PB/VA-CNT/CF (middle, red), and PB (bottom, blue). (For interpretation of the references to color in this figure legend, the reader is referred to the web version of this article.)

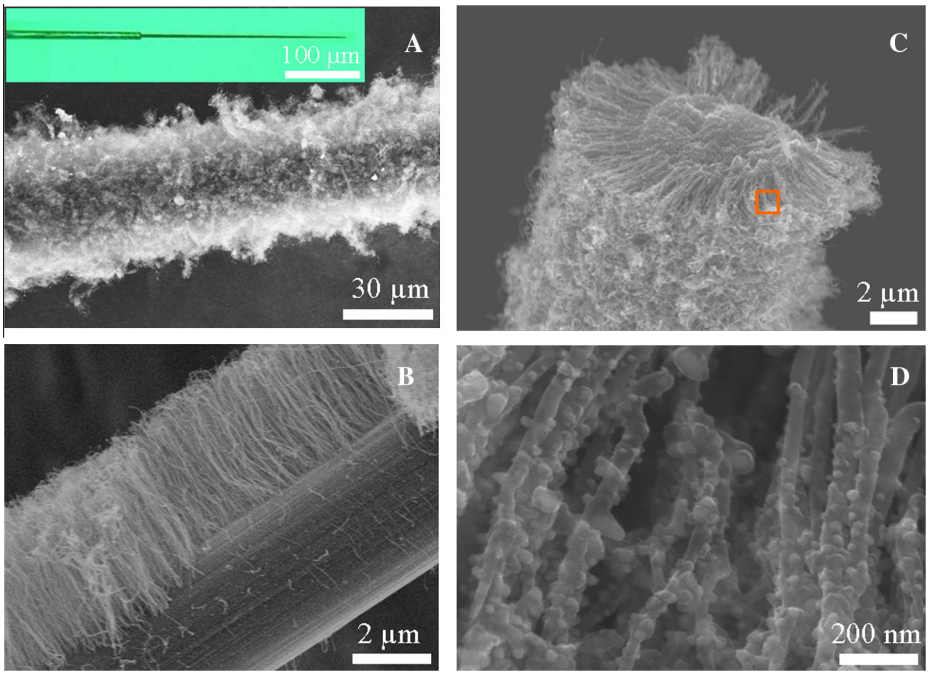

Fig. 4. (A and B) Top-down SEM images of the PB/VA-CNT/CFME. The inset in (A) shows Raman-imaging photography of as-prepared PB/VA-CNT/CFME. For (B), we elaborately scratched the PB/VA-CNT/CFME along its length for convenience to visualize the orientation of CNTs. (C) Cross-sectional SEM image of the tip of PB/VA-CNT/CFME. (D) High-resolution SEM image of the area in the square in (B).

designate, respectively, to the stretching mode of the CN functional group (υ_{CN}), and the Fe—C—N—Fe bending mode in the far-infrared region [23]. The weaker band at 1600 cm^{-1} is associated with O—H stretching due to interstitial water [23]. Further, the FT-IR spectrum for the PB/VA-CNT/CFME clearly records all these bands arising from both CNTs and PB nanoparticles, denoting the formation of the PB/CNT composite. Moreover, the υ_{CN} mode of the composite is negatively shifted by 60 cm^{-1} compared with that of PB alone; a similar significant shift is true in the far-infrared region, collectively revealing that a charge-transfer interaction between the components accompanies the formation of the PB/VA-CNT composite [18,19].

Fig. 5B shows the corresponding first-order Raman spectra for the VA-CNT/CF, PB/VA-CNT/CF, and PB nanoparticles. The VA-CNT/CF exhibits the characteristic disorder band (D-band, ~1290 cm^{-1}) and the tangential band (G-band, ~1500–1600 cm^{-1}) associated with graphites [24–26]. Furthermore, the PB nanoparticles generate Raman-scattering peaks at 2056 cm^{-1} and 2159 cm^{-1} from the stretching vibration of the CN group of PB [27]. Like the FT-IT spectra, the Raman spectra suggest that the deposition of PB on the CNTs is successful because all the characteristic bands for these two components are apparent after electrodeposition (the uppermost curve in Fig. 5B). Likewise, the relative increase in the sensitivity of the D-band versus the G-band, i.e., I_D/I_G, after the deposition of PB, indicates a strong interaction between the PB and the CNTs components, wherein the conjugated carbon atoms are slightly disrupted because simple physical adsorptions do not increase the disorder mode unless new defect sites are created in the procedure [26].

3.3. Detection of H_2O_2 and glucose

We infer the concentration of glucose by using the GOx/PB/VA-CNT/CFME to detect the H_2O_2 generated during the oxygen-involved enzymatic reaction. As illustrated in Scheme 1, the catalytic reduction of hydrogen peroxide at PB through a redox-reaction mechanism "relays" electrons from the active center of GOx to the substrate electrode [28]. Glucose biosensors of this kind are based on the successive reduction of oxygen to water via H_2O_2; hence, the selectivity of the electrode against the interference of oxygen is crucial in deciphering the signals correctly.

We subjected the PB/VA-CNT/CFME to selectivity test by comparing its voltammetric responses to the reductions of these two species. The reduction of H_2O_2 occurs with an overpotential about 0.22 V lower than that of the oxygen reduction reaction (ORR) (red curves, Fig. 6), indicating an excellent resistance against the latter reaction within a large range of potential. Conversely, the CNT/CFME without PB exhibits a higher potential (i.e., lower overpotential) of −0.18 V for the ORR than for the reduction of H_2O_2 (black curves, Fig. 6), so posing an essential barrier to detecting H_2O_2 by its reduction reaction. Those comparisons highlight the excellent selectivity of the PB/VA-CNT/CF that is directly linked to the peroxidase-like catalytic function of PB toward H_2O_2 reduction.

Fig. 6 also reveals a significant amplification in the sensitivity for the H_2O_2 reduction at the PB/VA-CNT/CFME in relation to the counterpart PB-free electrode. With an identical concentration of 2.0 mM H_2O_2, and under the same conditions, the PB/VA-CNT/CFME outputs a fourfold higher diffusion-current density than did the CNT/CFME, denoting the former's substantially improved electrocatalytic activity. Assuming that the electrodeposition of PB involved only an insignificant change in the geometrical surface area and considering the complicated pathways of H_2O_2 reduction, especially at CNT electrodes [29,30], we speculate that, for this specific reaction, the PB/VA-CNT/CFME might have a much more efficient electrochemical surface area than does the CNT/CFME due to their different reaction mechanisms. Most likely, the enzyme-catalytic reaction is free from interference from adsorption of intermediates or contaminants; comparatively, this is not the case for the direct reduction of H_2O_2 at the CNTs. This basic difference is amplified further by the electrode's structural alignment that allows many more reactive sites. Other explanations for the enhancement in the electrocatalytic activity of PB/CNT composites are based on the synergetic effect between the components [18,19]; however, convincing experimental evidences are needed to clarify these hypotheses.

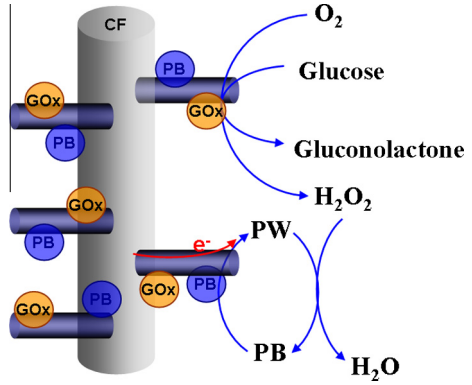

Scheme 1. Schematic illustration showing the redox cycles and electrochemical reactions occurring at the GOx/PB/VA-CNT/CFME to generate the analytical signal for detecting glucose. CF, carbon fiber; PB, Prussian blue; PW, Prussian white; GOx, glucose oxidase. (For interpretation of the references to color in this figure legend, the reader is referred to the web version of this article.)

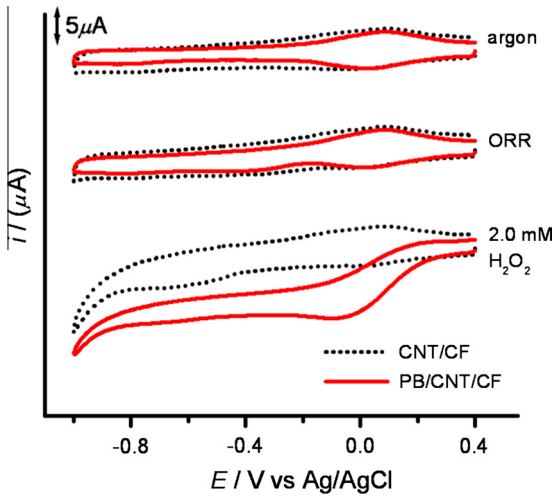

Fig. 6. CVs of oxygen reduction (middle) and H_2O_2 reduction (bottom) obtained at the PB/VA-CNT/CFME (solid, red), and the VA-CNT/CFME (dotted, black) at the scan rate of 50 mV s^{-1}. (For interpretation of the references to color in this figure legend, the reader is referred to the web version of this article.)

We tabulate in Table 1 the primary analytical properties of the two biosensors, *viz.* the PB/VA-CNT/CFME with and without GOx, for the amperometric measurement of H_2O_2 and glucose. To explore the essential functions of the aligned individual nanotubes, we used the GOx and PB co-modified carbon fiber microelectrode, i.e., GOx/PB/CFME and compared its chronoamperometric responses to glucose oxidation with that of the GOx/PB/VA-CNT/CFME (Fig. 7). The latter exhibits a sensitivity seven times higher than that of the GOx/PB/CFME (51.8 μA/mM versus 6.7 μA/mM), as shown in Table 1 and Fig. 7A. For both electrodes, we plot in Fig. 7B the loss of current as a function of time in responding to 5.0 mM glucose. There is insignificant change in the current from the GOx/PB/VA-CNT/CFME over 5 h of continuous *I–t* testing; in contrast, the response of the GOx/PB/CFME electrode severely

Table 1
Determination of H_2O_2 and glucose using the PB/VA-CNT/CFME and the PB/VA-CNT/CFME (without CNTs), respectively.[a]

	Detection limit (mmol/L)	Linearity range (mol/L)	Sensitivity (μA/mM)	Reproducibility (%RSD, $n = 8$)	Response time (s)
H_2O_2	5×10^{-6}	5×10^{-9}–2×10^{-2} $r^2 = 0.999$	51.8	<3%	<10
Glucose	0.05	5×10^{-5}–3.5×10^{-2} $r^2 = 0.998$	4.9	<5%	<10

[a] All the measurements were performed in 0.1 M phosphate solution (pH 6.5) at a polarized potential of −0.1 V versus Ag/AgCl (3.0 M KCl).

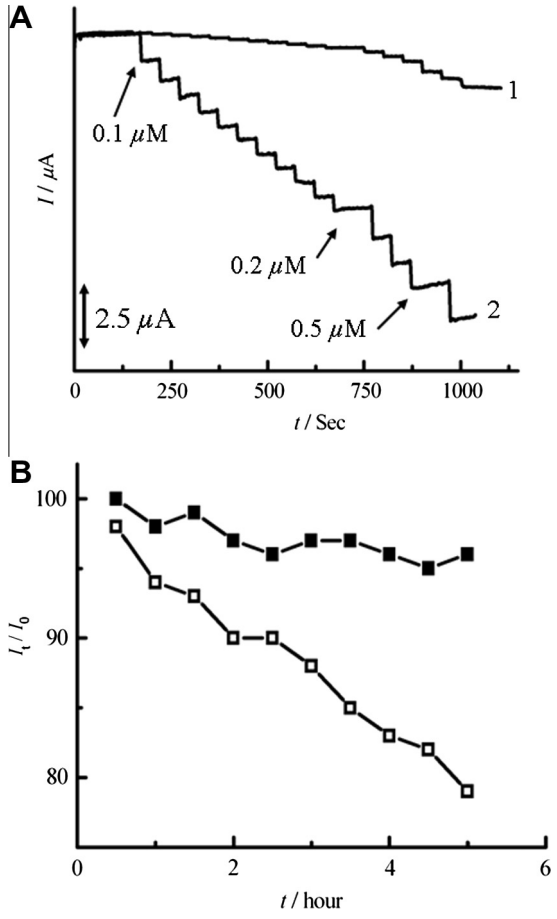

Fig. 7. (A) Amperometric *I*–*t* responses of the GOx/PB/CFME (curve 1) and the GOx/PB/VA-CNT/CFME (curve 2) at the potential of 0.0 V toward the successive addition of glucose while stirring PBS under ambient conditions. (B) Change in the amperometric response of the GOx/PB/CFME (empty, rectangle) and the GOx/PB/VA-CNT/CFME (solid, rectangle) to 5 mM glucose as a function of time. Stirring rate, 800 rpm.

declines, registering up to 23% loss of the initial current at the end of the experiment. Combining these findings with the SEM observations and the voltammetric- and spectroscopic-results, we consider that assembling the biomolecules and the nanoscale and microscale materials into a long-range-order heterojunction composite engenders novel functionalities, which are not evident in its single-component counterparts or in those with randomly mixed adducts. With all the nanotubes sited bottom-up on a curved plane of carbon fiber, the individual nanoelectrodes readily transports electrons along their lengths; the gaps between neighboring nanoelectrodes acted as hollow channels for the straightforward diffusion of substrates to access the enzyme molecules. These unique features, and those inherent in a low-dimensional electrode, might well expedite the chemical- and electrochemical-procedures for determining glucose at the VA-CNBEA.

4. Conclusions

In summary, we demonstrated the successful assembly of enzymes and CNTs and microfibers into a long-distance-order nanobioelectrode arrays that are notable for their ultra-sensitivity, low detection limit, and excellent stability in detecting glucose and hydrogen peroxide under a proximal biological condition. In addition to the intrinsic properties of individual components, their rational design toward an electrochemistry-defined hierarchical ordering plays a fundamental role in improving the biosensor's performance. Our methodology for preparing a nanobioelectrode array on microfibers may afford a new platform for devising biosensors and bioelectronics of major importance in clinic diagnosis- and healthcare-services.

Acknowledgments

Samsung Cheil Industries (San Jose, CA) was acknowledged for financial support. K.G. was in debt to Mohammed Ibrahim (ThermoFisher Scientific) for his helps in Raman measurements and analyses.

Appendix A. Supplementary material

Supplementary data associated with this article can be found, in the online version, at http://dx.doi.org/10.1016/j.jcis.2013.08.005.

References

[1] http://www.who.int/diabetes/en/.
[2] J. Wang, Chem. Rev. 108 (2008) 814–825.
[3] A. Heller, B. Feldman, Chem. Rev. 108 (2008) 2482–2505.
[4] A. Heller, B. Feldman, Acc. Chem. Res. 43 (2010) 963–973.
[5] E. Katz, I. Willner, J. Wang, Electroanalysis 16 (2004) 19–44.
[6] K. Gong, Y. Yan, M. Zhang, L. Su, S. Xiong, L. Mao, Anal. Sci. 21 (2005) 1383–1393.
[7] http://www.rcsb.org/pdb/home/home.do (see pdb77_1, May 2006, Molecule of the Month).
[8] F. Gao, L. Viry, M. Maugey, P. Poulin, N. Mano, Nat. Commun. 1 (2010) 2.
[9] P. He, L. Dai, Biomedical and Biomedical Nanotechnology: Carbon Nanotube Biosensors, vol. 6, Springer Science & Business Media LLC, New York, 2006.
[10] J. Wang, Electroanalysis 17 (2005) 7–14.
[11] A.A. Karyakin, E.E. Karyakina, L. Gorton, J. Electroanal. Chem. 456 (1998) 97–104.
[12] R.M. Wightman, Science 311 (2006) 1570–1574.
[13] K. Gong, M. Zhang, Y. Yan, L. Su, L. Mao, S. Xiong, Y. Chen, Anal. Chem. 76 (2005) 6500–6505.
[14] L. Qu, Y. Zhao, L. Dai, Small 2 (2006) 1052–1059.
[15] L. Mao, J. Jin, L. Song, K. Yamamoto, L. Jin, Electroanalysis 11 (1999) 499–504.
[16] D. Moscone, D. D'Ottavi, D. Compagnone, G. Palleschi, Anal. Chem. 73 (2001) 2529–2535.
[17] Z. Li, J. Chen, W. Li, K. Chen, L. Nie, S. Yao, J. Electroanal. Chem. 603 (2007) 59–66.
[18] J. Li, J. Qiu, J. Xu, H. Chen, X. Xia, Adv. Funct. Mater. 17 (2007) 1574–1580.
[19] Y. Zhang, Y. Wen, Y. Liu, D. Li, J. Li, Electrochem. Commun. 6 (2004) 1180–1184.
[20] D. Zhang, K. Wang, D. Sun, X. Xia, H. Chen, Chem. Mater. 15 (2003) 4163–4165.
[21] S.S. Kumar, J. Joseph, K.L. Phani, Chem. Mater. 19 (2007) 4722–4730.
[22] H. Hu, Y. Chen, A.M. Rao, P.C. Eklund, R.C. Haddon, Science 282 (1998) 95–98.
[23] P.J. Kulesza, M.A. Malik, A. Denca, J. Strojek, Anal. Chem. 68 (1996) 2442–2446.
[24] S. Maldonado, K.J. Stevenson, J. Phys. Chem. B 109 (2005) 4707–4716.
[25] M.S. Dresselhaus, G. Dresselhaus, A. Jorio, J. Phys. Chem. C 111 (2007) 17887–17893.
[26] C.A. Dyke, J.M. Tour, Chem. Eur. J. 10 (2004) 812–817.
[27] L. Xia, R.L. McCreery, J. Electrochem. Soc. 146 (1999) 3696–3701.
[28] J. Wang, J. Liu, L. Chen, F. Lu, Anal. Chem. 66 (1994) 3600–3603.
[29] Y. Tian, B.L. Allen, D.R. Kauffman, A. Star, J. Am. Chem. Soc. 131 (2009) 13200–13201.
[30] K. Gong, S. Chakrabarti, L. Dai, Angew. Chem. Int. Ed. 47 (2008) 5446–5450.